

The Neutrino Opacity of Neutron Star Inner Crust

P. N. Alcain and C. O. Dorso

*Departamento de Física, FCEyN, UBA and IFIBA, Conicet,
Pabellón 1, Ciudad Universitaria, 1428 Buenos Aires, Argentina and
IFIBA-CONICET*

(Dated: March 31, 2016)

Background: In neutron stars the nucleons are submitted to extreme conditions. The study of this natural occurring objects can lead to further understanding of the behaviour of nuclear matter in highly asymmetric nuclei. Among the characteristics of neutron stars, the neutrino opacity of the crust — associated to structural inhomogeneities — stands out as one of the possible magnitudes linked to an observable.

Purpose: We have carried out a systematic study of this neutrino opacity for different thermodynamic conditions in order to assess the impact that the structure has on it.

Method: We study the dynamics of the neutrino opacity by the heterogeneous crust at different thermodynamics conditions according to the neutron star crust with a semiclassical molecular dynamics model. For different densities, proton fractions and temperature, we calculate the very long range opacity and the cluster distribution.

Results: Being the neutrino emission the main mechanism for neutron stars cooling down, the neutrino opacity is of crucial importance. We found its maximum value for temperatures and densities low compared with the inner crust, and a proton fraction close to the symmetric case $x = 0.5$.

Conclusions: Within the used model, the neutrinos are absorbed mostly close to the surface of the neutron star. Also, for high temperatures, a large cluster still exists, but the appearance of several small-sized clusters smears out the very long range order needed for neutrino opacity.

PACS numbers: PACS 24.10.Lx, 02.70.Ns, 26.60.Gj, 21.30.Fe

I. INTRODUCTION

A neutron star is an astronomical object with a radius of approximately 10 km and a mass of about a few solar masses. Its structure can be divided in two parts, according to current models [1, 2]: the *crust*, about 1.5 km thick and with a density of up to half the normal nuclear density ρ_0 ; and the *core*, where the structure is still unknown and remains highly speculative [3]. Ravenhall *et al.* in Ref. [4] and Hashimoto *et al.* in Ref. [5] proposed that the neutron star crust is composed by the structures known as *nuclear pasta*, as we shall explain later on.

Most neutron stars are supernovae remnants, that happen when the hot and dense iron core of a dying massive star (known as *proto-neutron star*) collapses. During the collapse, several nuclear processes take place in the inner core of the star — electron capture, photodisintegration, Urca, etc. These processes have a twofold consequence: not only they largely increase the overall neutron number of the system, but also produce a large amount of neutrinos. These neutrinos flow outward, and its emission is the main mean by which the neutron stars cool down. Therefore, the interaction between the neutrinos and neutron star matter is key to comprehend two aspects of a neutron star history: its genesis and its thermal evolution, once formed. The interaction between the neutrinos streaming from the core of the proto-neutron star and its outer layers also plays an important role in reversing the collapse that causes the supernova.

The neutron stars is composed of neutrons and protons embedded in a degenerate electron gas. Protons and neutrons in the crust are supposedly arranged in struc-

tures that differ substantially from the “normal” nuclei — the non-homogeneous phases collectively known as *nuclear pasta*. The structure of this nuclear pasta is linked to the neutrino opacity of neutron stars crust, neutron star quakes, and pulsar glitches. Specifically, the neutron star quakes and pulsar glitches are related to the mechanical properties of the crust matter [6], while the neutrino opacity is due to its morphological properties. The enhancement of the crust’s opacity is because of the coherent scattering, related to the neutron-neutron static structure factor of nuclear pasta, according to Ref. [7]:

$$\frac{d\sigma}{d\Omega} = \left(\frac{d\sigma}{d\Omega} \right)_{\text{neutron}} \times S(q).$$

And since neutron star cooling is associated with neutrino emission from the core, the interaction between the neutrinos and the particular structure of the crust would dramatically affect the thermal history of young neutron stars. These neutrinos are produced mainly due to modified Urca processes:

$$p + n + e \rightarrow n + n + \nu_e$$

Several models have been developed to study nuclear pasta, and they have shown that these structures arise due to the interplay between nuclear and Coulomb forces in an infinite medium. Nevertheless, the dependence of the observables on different thermodynamic quantities has not been studied in depth. The original works of Ravenhall *et al.* [4] and Hashimoto *et al.* [5] used a compressible liquid drop model, and have shown that the now

known as *pasta phases* –*lasagna*, *spaghetti* and *gnocchi*– are solutions to the ground state of neutron star matter. From then on, different approaches have been taken, that we roughly classify in two categories: mean field or microscopic.

Mean field works include the Liquid Drop Model, by Lattimer *et al.* [1], Thomas–Fermi, by Williams and Koonin [8], among others [9–14]. Microscopic models include Quantum Molecular Dynamics, used by Maruyama *et al.* [15, 16] and by Watanabe *et al.* [17], Simple Semi-classical Potential, by Horowitz *et al.* [18] and Classical Molecular Dynamics, used in our previous works [19].

In some recent studies, phases different from the typical *nuclear pasta* were found. The work by Nakazato *et al.* [14], inspired by polymer systems, found also gyroid and double-diamond structures, with a compressible liquid drop model. Dorso *et al.* [19] arrived to pasta phases different from those already mentioned with molecular dynamics, studying mostly its characterization at very low temperatures. In our previous work [20] we have shown that these new pasta phases had an absorption peak in the characteristic wavelength of the Urca neutrinos for symmetrical neutron star matter. All these non homogeneous phases add up to what we shall call *Generalized Nuclear Pasta* (GNP).

Of the many models used to study neutron stars, the advantages of classical or semiclassical models are the accessibility to position and momentum of all particles at all times and the fact that no specific shape is hard-coded in the model, as happens with most mean field models. This allows the study of the structure of the nuclear medium from a particle-wise point of view. Many models exist with this goal, like quantum molecular dynamics [15], simple-semiclassical potential [18] and classical molecular dynamics [21]. In these models the Pauli repulsion between nucleons of equal isospin is either hard-coded in the interaction or as a separate term [22].

In the works done by Horowitz *et al.* [7, 18], the neutrino absorption and mean free path was calculated for a specific temperature and proton fraction. With these results, they showed that from models with long-range Debye-like repulsion and short-range nuclear-like interaction can emerge a very long range structure, the *nuclear pasta*. For the studied system, this very long range structure has an absorption peak in the energy region of Urca neutrinos.

In this work, we build up on this result for a different model with the same qualitative characteristics, also extending the studied thermodynamic region for different proton fractions, temperatures and densities. We calculate the opacity for large wavelengths compared to the interparticle distance of nuclear matter ($r_{nn} \approx 1.8$ fm) and the cluster distribution. In section II we introduce the model and the cluster recognition tools that we used to analyze the results. Section III A shows the cluster distribution for different configurations, and in section III B we study in greater detail the opacity of the pasta to long range neutrinos, for different thermodynamic pa-

rameters.

II. CLASSICAL MOLECULAR DYNAMICS

In this work, we study GNP with the classical molecular dynamics model CMD. It has been used in several heavy-ion reaction studies to: help understand experimental data [23]; identify phase-transition signals and other critical phenomena [24–28]; and explore the caloric curve [29] and isoscaling [30, 31]. CMD uses two two-body potentials to describe the interaction of nucleons, which are a combination of Yukawa potentials:

$$V_{np}^{\text{CMD}}(r) = v_r \exp(-\mu_r r)/r - v_a \exp(-\mu_a r)/r$$

$$V_{nn}^{\text{CMD}}(r) = v_0 \exp(-\mu_0 r)/r$$

where V_{np} is the potential between a neutron and a proton, and V_{nn} is the repulsive interaction between either *nn* or *pp*. The cutoff radius is $r_c = 5.4$ fm and for $r > r_c$ both potentials are set to zero. The Yukawa parameters μ_r , μ_a and μ_0 were determined to yield an equilibrium density of $\rho_0 = 0.16 \text{ fm}^{-3}$, a binding energy $E(\rho_0) = 16 \text{ MeV/nucleon}$ and a compressibility of 250 MeV.

To simulate an infinite medium, we used this potential with $N = 5500$ particles under periodic boundary conditions, with different proton fraction (i.e. with $x = Z/A = 0.1 < x < 0.5$) in cubical boxes with sizes adjusted to have densities between $\rho = 0.001 \text{ fm}^{-3} \leq \rho \leq 0.08 \text{ fm}^{-3}$. This simulations have been done with LAMMPS [32], using its GPU package [33].

A. Coulomb interaction in the model

Since a neutralizing electron gas embeds the nucleons in the neutron star crust, the Coulomb forces among protons are screened. The model we used to model this screening effect is the Thomas–Fermi approximation, used with various nuclear models [7, 15, 19]. According to this approximation, protons interact via a Yukawa-like potential, with a screening length λ :

$$V_{TF}(r) = q^2 \frac{e^{-r/\lambda}}{r}.$$

Theoretical estimates for the screening length λ are $\lambda \sim 100$ fm [34], but we set the screening length to $\lambda = 20$ fm. This choice was based on previous studies [35], where we have shown that this value is enough to adequately reproduce the expected length scale of density fluctuations for this model, while larger screening lengths would be a computational difficulty. We analyze the opacity to neutrinos of the structures for different proton fractions and densities.

B. Cluster recognition

In typical configurations we have not only the structure known as nuclear pasta, also a nucleon gas that surrounds the nuclear pasta. In order to properly characterize the pasta phases, we must know which atoms belong to the pasta phases and which belong to this gas. To do so, we have to find the clusters that are formed along the simulation.

One of the algorithms to identify cluster formation is Minimum Spanning Tree (MST). In MST algorithm, two particles belong to the same cluster $\{C_n^{\text{MST}}\}$ if the relative distance of the particles is less than a cutoff distance r_{cut} :

$$i \in C_n^{\text{MST}} \Leftrightarrow \exists j \in C_n \mid r_{ij} < r_{\text{cut}}$$

This cluster definition works correctly for systems with no kinetic energy, and it is based in the attractive tail of the nuclear interaction. However, if the particles have a non-zero temperature, we can have a situation of two particles that are closer than the cutoff radius, but with a large relative kinetic energy.

To deal with situations of non-zero temperatures, we need to take into account the relative momentum among particles. One of the most sophisticated methods to accomplish this is the Early Cluster Recognition Algorithm (ECRA) [36]. In this algorithm, the particles are partitioned in different disjoint clusters C_n^{ECRA} , with the total energy in each cluster:

$$\epsilon_n = \sum_{i \in C_n} K_i^{\text{CM}} + \sum_{i,j \in C_n} V_{ij}$$

where K_i^{CM} is the kinetic energy relative to the center of mass of the cluster. The set of clusters $\{C_n\}$ then is the one that minimizes the sum of all the cluster energies $E_{\text{partition}} = \sum_n \epsilon_n$.

ECRA algorithm can be easily used for small systems [37], but being a combinatorial optimization, it cannot be used in large systems. While finding ECRA clusters is very expensive computationally, using simply MST clusters can give extremely biased results towards large clusters. We have decided to go for a middle ground choice, the Minimum Spanning Tree Energy (MSTE) algorithm [19]. This algorithm is a modification of MST, taking into account the kinetic energy. According to MSTE, two particles belong to the same cluster $\{C_n^{\text{MSTE}}\}$ if they are energy bound:

$$i \in C_n^{\text{MSTE}} \Leftrightarrow \exists j \in C_n : V_{ij} + K_{ij} \leq 0$$

While this algorithm doesn't yield the same theoretically sound results from ECRA, it still avoids the largest pitfall of naïve MST implementations for the temperatures used in this work. To illustrate this concept, we show in figure 1 the relative kinetic energy of pairs that are bound by MST algorithm, with $r_{\text{cut}} = 5.4$ fm, for a system with $x = 0.5$, $\rho = 0.04 \text{ fm}^{-3}$, $T = 1.0$ MeV. We can

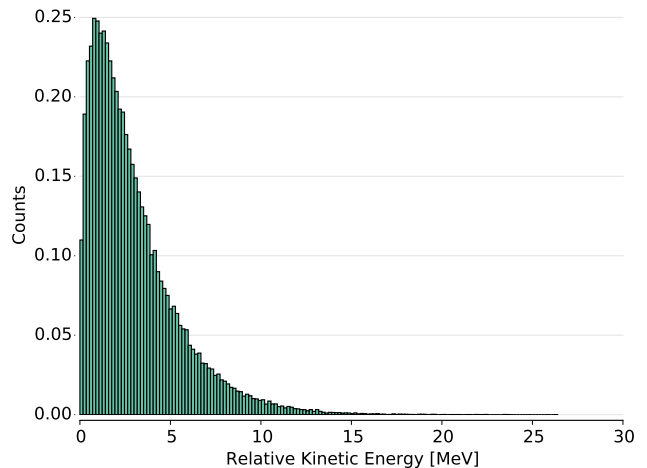


Figure 1: (Color online) Relative kinetic energy for pairs inside MST clusters.

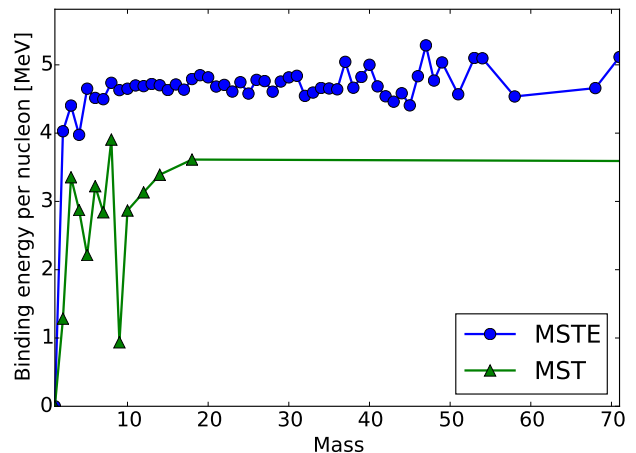


Figure 2: (Color online) Binding energy for MST and MSTE clusters. We can see that for every cluster size, MSTE clusters are more bound than MST ones.

see that a considerable amount of pairs have a relative energy larger than 5 MeV.

Even further, for systems of density $\rho = 0.01 \text{ fm}^{-3}$ and proton fraction $x = 0.3$ with the lowest temperature studied ($T = 0.5$ MeV), we tallied the binding energy per nucleon E_B for the different cluster mass (this is related to the ϵ_n from the ECRA definition: $E_B = -\epsilon_n/m_n$, with m the mass of the cluster C_n) that appeared along the different snapshots. This was done both for MST and MSTE clusters, and the obtained results are in figure 2. In this figure we can see that for every cluster size, MSTE clusters have a larger binding energy than MST clusters.

III. RESULTS AND DISCUSSION

A. Clusters

In figure 3 we show four different snapshots for proton fractions of $x = 0.4$ and $x = 0.5$ and temperature $T = 0.5$ MeV and $T = 1.0$ MeV. In it we clearly see that the structures are no longer limited to those originally proposed by Ravenhall *et al.* [4]. To study them further we can see in figure 4 the corresponding cluster distribution according to MSTE algorithm. In this figure, we can see that for a proton fraction $x = 0.2$ there are many isolated nucleons that are almost exclusively neutrons. These work as a neutron gas that embeds the underlying proton structure.

Another consequence of the neutron gas is that the proton fraction of the GNP structure is slightly higher than the proton fraction in the simulation cell. We can see from figure 4 that the proton fraction in the large cluster is of about $x = 0.24$, while the macroscopic proton fraction is $x = 0.2$. From figure 5 we can see the mass of the largest cluster, and note that even for very high temperatures ($T = 2.0$ MeV) a large cluster appears for every proton fraction. In particular, the smallest of the largest clusters contains more than 50% of the total mass of the system.

B. Neutrino Opacity

To find the opacity of this kind of heterogeneous matter we calculated the structure factor of the system for a broad range of wavelengths of interest related to the pasta structure, and then search for the maximum. To take a glimpse at the mass distribution of the system we calculate the pair distribution function of the neutrons $g_{nn}(r)$, which is related to the number of neutrons at a distance r away from a given neutron, in a shell of thickness dr :

$$dn = \frac{N}{V} g_{nn}(r) 4\pi r^2 dr$$

of which the structure factor $S(q)$ is the Fourier transform:

$$S_{nn}(q) = 1 + \rho \int_V dr e^{-iqr} g_{nn}(r)$$

This expression is for an angle averaged $S(q)$, since collapsing cores are polycrystalline, and the orientation of each grain of the crystal is randomly oriented [39]. Figure 6 shows the pair distribution function and structure factor (see appendix for a detailed explanation of its calculation) for a system with proton fraction $x = 0.5$, density $\rho = 0.05 \text{ fm}^{-3}$ and temperature $T = 0.5$ MeV. In the pair distribution function we can identify (marked with \blacktriangledown) the peak that belongs to the crystalline structure of

the nucleons within the pasta — neutron correlation with nearest neighbors —, and also a very long range interaction (marked with a dashed line $- -$); this interaction translates to the peak for low wave-numbers in the structure factor, related to the pasta structures. The structure factor displays a peak located at $q_{\text{peak}} = 0.43 \text{ fm}^{-1}$ with a width of about $\text{FWHM} = 0.08 \text{ fm}^{-1}$, thus defining a range of wavelengths in which the structure is considerably opaque.

For each configuration of given proton fraction, density and temperature, we calculate the structure factor and extract the pasta peak of the structure factor for long wavelengths. We will refer to this value as “Absorption of the system”.

We simulated the system for a total of about 1000 different configurations (4 different proton fractions, 10 different densities and 30 different temperatures). For each combination of (x, ρ, T) we calculate the pair distribution function $g(r)$, whose Fourier transform is the structure factor. From this structure factor we take the very long range peak. A word of caution must be said about the low temperatures. As we have shown in a previous work [20], below a certain temperature (near 1 MeV) the system might freeze in one of many local minima. Because of this, the system cannot be directly simulated at low temperatures. Instead, the low temperature limit must be obtained coming from high temperatures, carefully lowering the temperature and checking whether the system thermalized or not.

Figure 7 shows the wavelength and height of the “absorption” peak for the lowest temperature studied in this work ($T = 0.5$ MeV) as a function of the density. We observe that the wavelength decreases as the density increases, meaning that the correlation length of the structure is lower as the density increases. This is to be expected, since the higher the density, the closer the structures are. Nevertheless, we emphasize that the structure changes with the density, not only with transition in morphology (e. g. from *spaghetti* to *lasagna*) but also, for example, *gnocchi* clusters have different sizes for different densities. This interplay between the structures changing internally and also changing its spatial distribution is what results in the figure 7a. We can see that the wavelength for maximum opacity changes rapidly for low densities (those of *gnocchi*), but tends to stabilize for the other pasta phases. Consider also that, since the $S(q)$ has a certain width near the peak, the structure would absorb neutrinos in a range of wavelengths that are near said maximum. Interestingly, the “absorption peak” height reaches its maximum for $\rho = 0.01 \text{ fm}^{-3}$, where we still have *gnocchi* as can be evidenced by the cluster distributions in figure 8.

In figure 9 we show the “Absorption of the system” for the different thermodynamical configurations. We can see there that as the proton fraction decreases, the absorption decreases as well. For every proton fraction studied, the absorption peak falls rapidly for temperatures higher than $T = 0.8$ MeV, and it is about $1/4$ of

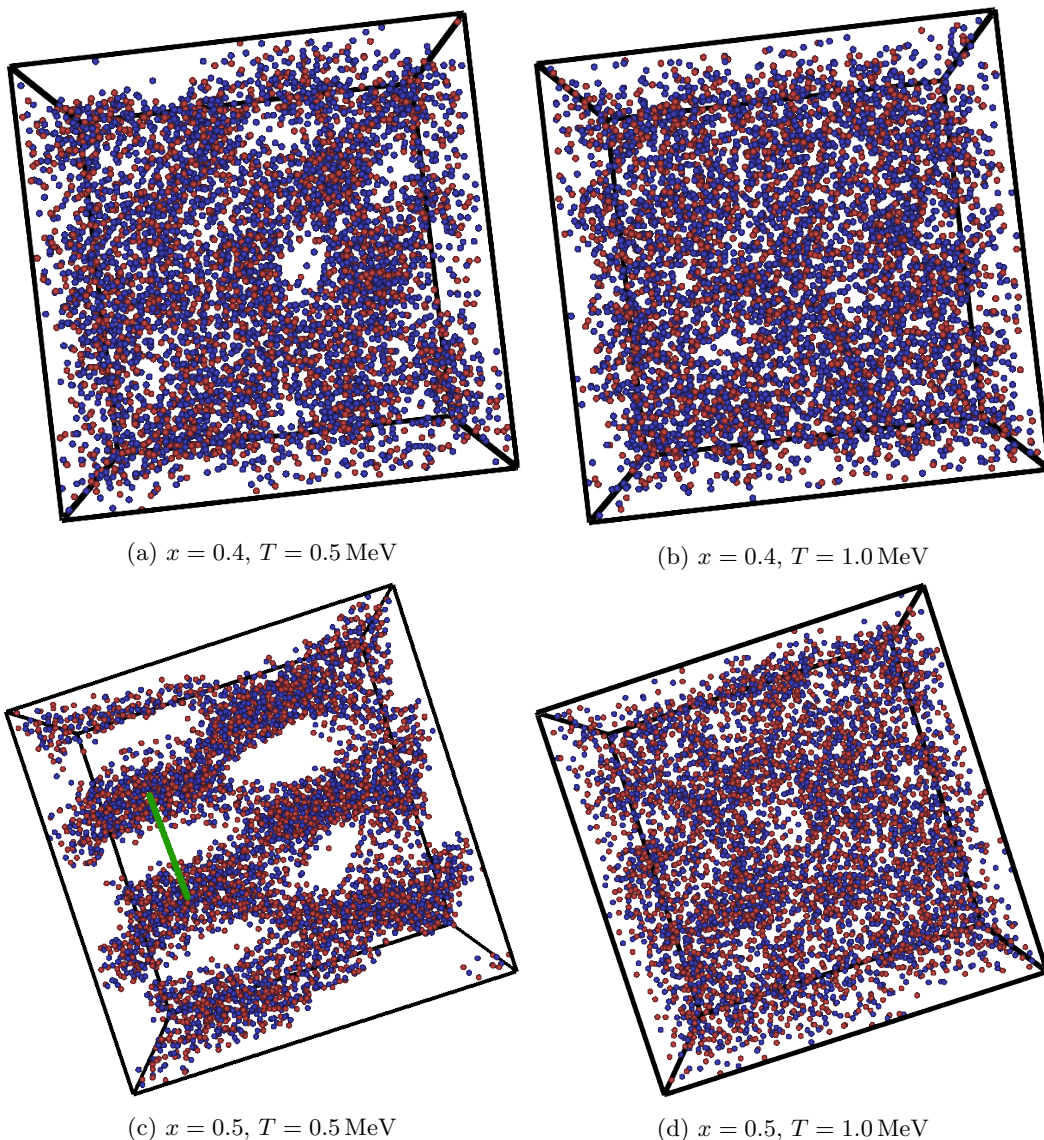


Figure 3: (Color online) Snapshots of a system with density $\rho = 0.04 \text{ fm}^{-3}$ for different values of proton fraction and temperature, generated with VisIt [38]. Structures obtained at $T = 0.5 \text{ MeV}$ differ substantially. Nevertheless both show inhomogeneities. We can see in panel 3c a green line marking a correlation length of $\approx 15 \text{ fm}$.

the peak absorption at $T = 0.5 \text{ MeV}$. The reason why as the proton fraction is reduced, so does the absorption can be understood in this way: the backbone structure is due to the proton long-range Coulomb interaction. When there is one neutron for each proton ($x = 0.5$), the neutron structure follows almost identically that of the proton backbone. However, as the neutron proportion rises, the neutron structure is smeared out and its long range correlation begins to vanish. This effect can be seen in the cluster distribution for $x = 0.2$, where we have many isolated neutrons, that are the embedding neutron gas. These characteristics affect the inhomogeneities that appear in $x = 0.5$, suppressing its long range absorption.

From figure 5 we can see that even for very high temperatures ($T = 2.0 \text{ MeV}$) a large cluster appears for every

proton fraction. This large structure is the *Generalized Nuclear Pasta*, that is responsible for the long range interaction. The reason why the opacity gets drastically depressed as the temperature rises therefore is not because the large cluster disappears, but because of structural changes.

IV. DISCUSSION AND CONCLUDING REMARKS

According to neutron stars models [1], as we get deeper into the neutron star: the proton fraction gets lower; the temperature gets higher; and the density gets higher too. Therefore, according to the current model, the opacity

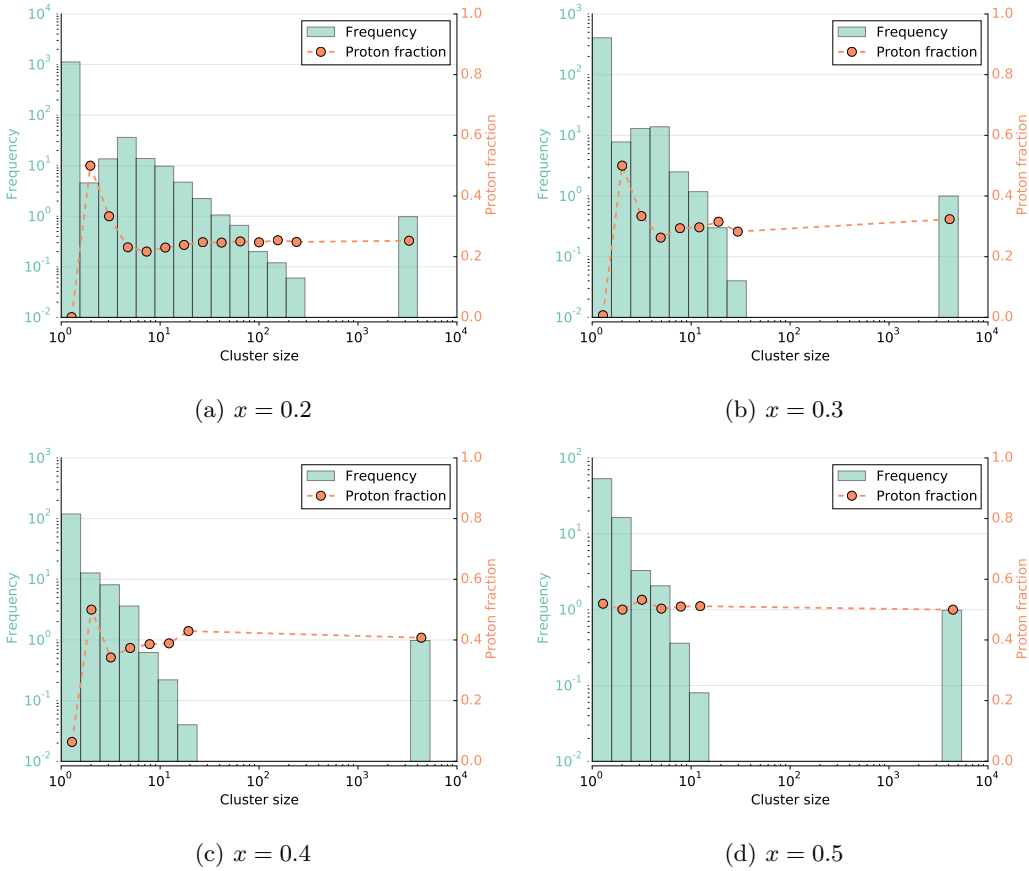


Figure 4: (Color online) Cluster distribution with MSTE algorithm for temperature $T = 2.0$ MeV, density $\rho = 0.04 \text{ fm}^{-3}$ and different proton fractions. For the lowest of the studied proton fractions, $x = 0.2$, the large cluster has a higher proton fraction (about 30% higher) and there are many isolated neutrons. Please note that the scales are different for each graph.

to neutrinos decreases rapidly as we go towards the neutron star core. This means that the neutrino absorption is produced mostly close to the surface of the neutron star. We also found structures that are not those originally proposed, and cataloged as *lasagna*, *spaghetti* and *gnocchi*, as can be seen in figure 3. Further analysis of the cluster distribution shows that for high temperatures, although there is no absorption in the neutrinos wavelength, a large cluster appears. This absence of opacity is because the system approaches the homogeneous limit.

We expect these results to be qualitatively correct, but quantitatively dependent on the model chosen to describe the neutron star crust. The model we are using in this work has been extensively studied in collisions and heavy ion physics, that is the reason why we have chosen it to describe quantitatively neutron star matter.

Neutron star hydrodynamical models [2, 3, 40–42] yield proton fraction, density and temperature profiles in the neutron star, as a function of the radius. From this work, we are able to find, for this specific model, the neutrino absorption for different thermodynamic conditions. Therefore, combining these two results with even-

tual measurements of the neutrino absorption in neutron stars, we can check the validity of different nuclear models and, consequently, move a step forward towards finding the nuclear equation of state.

Appendix: On the calculation of the structure factor

The structure factor of a system is defined from the *sample scattering amplitude* [43]

$$\Psi(\mathbf{Q}) = \frac{1}{\langle b \rangle} \sum_i b_i e^{i\mathbf{Q} \cdot \mathbf{R}_i} \quad (\text{A.1})$$

with \mathbf{Q} the diffraction vector or momentum transfer. \mathbf{R}_i is the position of the particle i , and $\langle b \rangle$ is the average of the scattering amplitude of each particle in the vacuum b_i . From this moment on, we will consider that all of the atoms are of the same species, $b_i = b$.

From $\Psi(\mathbf{Q})$ we define the structure factor $S(\mathbf{Q})$ as

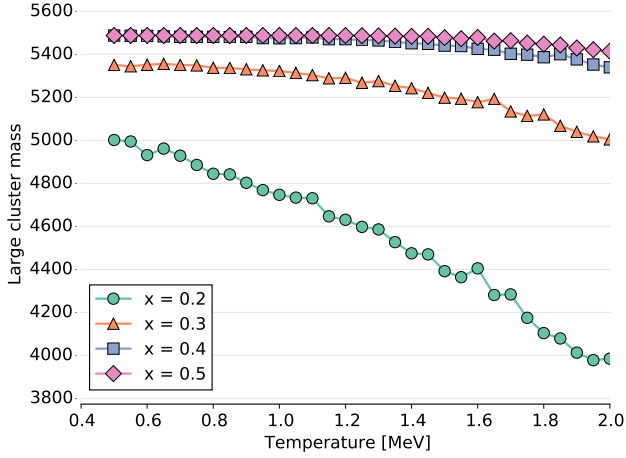


Figure 5: (Color online) Mass of the largest cluster for $\rho = 0.04 \text{ fm}^{-3}$ for different values of x .

$$S(\mathbf{Q}) = \frac{1}{N} |\Psi(\mathbf{Q})|^2$$

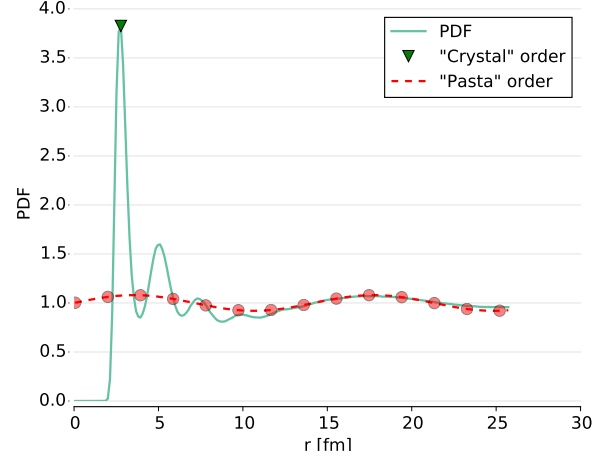
What follows *immediately* from this expression is that the structure function must be always positive for every value of \mathbf{Q} . We can expand the scattering amplitude and use $|z| = z \cdot z^*$ and, if all the atoms are of the same type,

$$\begin{aligned} S(\mathbf{Q}) &= \frac{1}{N} \left(\sum_i e^{i\mathbf{Q} \cdot \mathbf{R}_i} \right) \left(\sum_j e^{-i\mathbf{Q} \cdot \mathbf{R}_j} \right) \\ &= \frac{1}{N} \sum_{i,j} e^{i\mathbf{Q} \cdot (\mathbf{R}_i - \mathbf{R}_j)} \\ &= \frac{1}{N} \left[N + \sum_{i < j} \left(e^{i\mathbf{Q} \cdot (\mathbf{R}_i - \mathbf{R}_j)} + e^{i\mathbf{Q} \cdot (\mathbf{R}_j - \mathbf{R}_i)} \right) \right] \\ &= 1 + \frac{2}{N} \sum_{i < j} \cos \mathbf{Q} \cdot \mathbf{R}_{ij} \end{aligned}$$

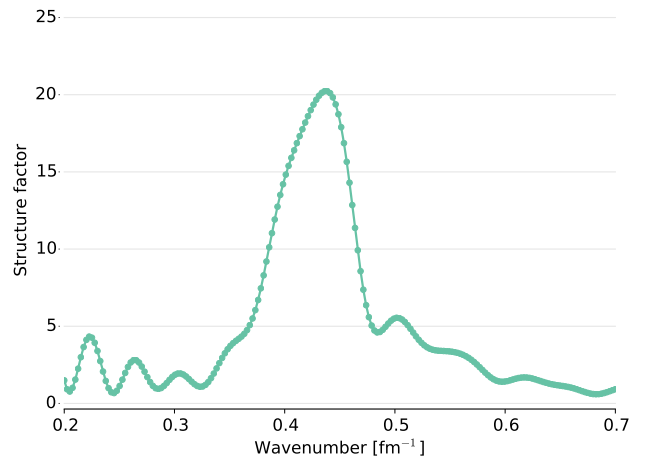
Usually we are interested in the *powder average* of the structure factor. This is the structure factor averaged for every possible orientation of the diffraction vector - because in a powder we have a lot of structures randomly oriented. We calculate therefore

$$S(q) = \frac{1}{4\pi} \int d\phi d(\cos \theta) S(\mathbf{Q})$$

This integral can be performed easily if we put the z axis along with the direction of \mathbf{Q} and perform the integration rotating the distances \mathbf{R}_{ij}



(a) Pair distribution function.



(b) Static structure factor.

Figure 6: (Color online) 6a Pair distribution function and 6b static structure factor for a system with proton fraction $x = 0.4$, density $\rho = 0.04 \text{ fm}^{-3}$ and temperature $T = 0.5 \text{ MeV}$.

The first peak in the $g(r)$ due to crystalline structures is marked with \blacktriangledown , while the very long range order is marked with a dashed line $- -$. In the structure factor we can see the peak located at $q_{\text{peak}} = 0.43 \text{ fm}^{-1}$ with a width of about $\text{FWHM} = 0.08 \text{ fm}^{-1}$. The ripples for low wavenumbers are due to finite size effects.

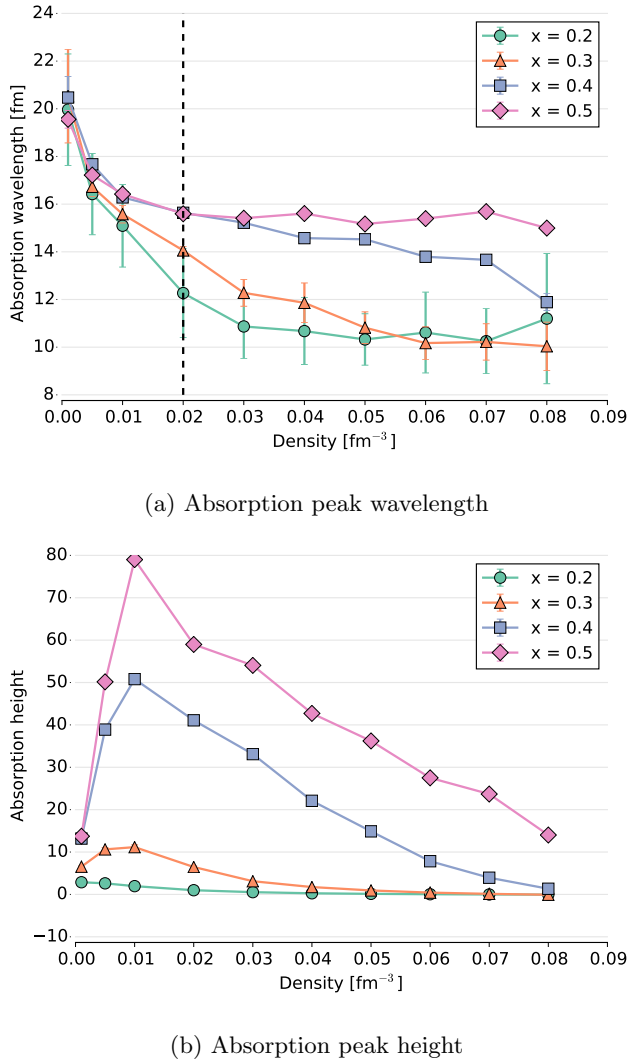


Figure 7: (Color online) Absorption peak 7a wavelength and 7b height for low temperature ($T = 0.5$ MeV) as a function of density for different proton fractions. We can see the wavelength changing rapidly for $\rho < 0.02 \text{ fm}^{-3}$ (*gnocchi* phase) and stabilizing for higher densities.

$$\begin{aligned}
 S(q) &= \frac{1}{4\pi} \int d\phi d(\cos \theta) \left[1 + 2 \sum_{i < j} \cos(q r_{ij} \cos \theta) \right] \\
 &= 1 + \frac{1}{2N} \int d(\cos \theta) 2 \sum_{i < j} \cos(q r_{ij} \cos \theta) \\
 &= 1 + \frac{1}{2N} 2 \sum_{i < j} \frac{\sin(q r_{ij} u)}{q r_{ij}} \Big|_{u=-1}^{u=1} \\
 &= 1 + \frac{2}{N} \sum_{i < j} \frac{\sin(q r_{ij})}{q r_{ij}}
 \end{aligned}$$

This is the famous Debye formula and, since its the

average of an always positive quantity, it must be always positive.

One of the most usual problems when we model and study systems in computer simulations is that we don't have actual *infinite* systems. We do, however, use the periodic boundary conditions (PBC) usually to emulate the behavior of infinite systems. With the periodic boundary conditions we use the minimum image convention: from all the possible positions through the boundaries for particle i and j , whichever pair is closest. Using with the above mentioned method for a very simple test case (a simple cubic 3D lattice with $4 \times 4 \times 4 = 64$ atoms) we calculated the structure factor that can be seen in figure 10.

We can see that the structure factor calculated with PBC attains negative values, even though those values ought to be forbidden. The reason for this behaviour is the minimum image convention: the pair distance now isn't always $r_{ij} = r_j - r_i$, but depends on whether we use the original particles or their images. Therefore, this "new" structure factor isn't the product of two conjugate complex numbers[44]. To explore the effect that the minimum image convention has on the structure factor, we have a comparison of the structure factor with and without boundary conditions (i. e., with the 64 atoms in a void) in figure 10.

This shows that the structure factor, when we use its definition *without minimum image convention*, is (as expected) always positive.

The question then, remains: how can we simulate an infinite medium when calculating structure factor? The first answer is that it is not that obvious that we would actually need this *infinite* medium, since the periodic images of the cell would be aligned in a crystal that might interfere with the structure within the cell — the one we actually do want to study. However, a couple of replicas should be enough to smear out the finite size effects. One of the possibilities is to replicate explicitly the box, creating the particles in the neighboring cells by duplication of the original ones. This, though, implies a calculation much harder, since the sum is over N^2 particles, and replicating only one cell right and left in each direction would imply a computational time of $(3^3 \cdot N)^2 \approx 700 \cdot N^2$. In general, the complexity $\mathcal{O}(N^2)$ makes structure factor calculation very expensive for large systems.

There is an alternative to add the boundary conditions. We begin with the definition of the *sample scattering amplitude* as in A.1, but writing explicitly the periodic boundary images we want to consider:

$$\Psi(\mathbf{Q}) = \sum_i \sum_j e^{i\mathbf{Q} \cdot (\mathbf{R}_i + \mathbf{\Delta L}_j)} \quad (\text{A.2})$$

where $\mathbf{\Delta L}_j$ is the distance between a particle and its j -th periodic replica. Since the sums are independent, we can write:

$$\Psi(\mathbf{Q}) = \left(\sum_i e^{i\mathbf{Q} \cdot \mathbf{R}_i} \right) \left(\sum_j e^{i\mathbf{Q} \cdot \mathbf{\Delta L}_j} \right) \quad (\text{A.3})$$

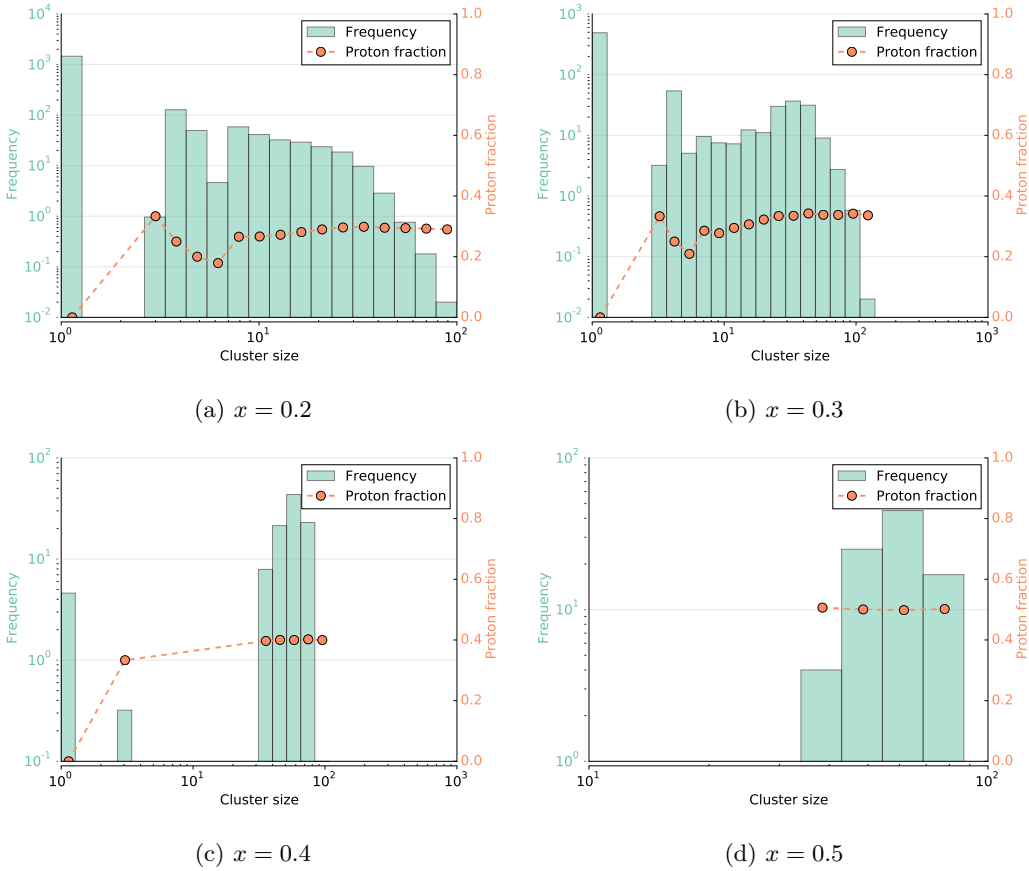


Figure 8: (Color online) Cluster distribution with MSTE algorithm for temperature $T = 0.5$ MeV, density $\rho = 0.01 \text{ fm}^{-3}$ and different proton fractions. We can see that all of them have *gnocchi* mass distributions. Please note that the scales are different for each graph.

Multiplying by the conjugate gives us the structure factor

$$S(\mathbf{Q}) = \left| \sum_i e^{i\mathbf{Q} \cdot \mathbf{R}_i} \right|^2 \left| \sum_j e^{i\mathbf{Q} \cdot \Delta \mathbf{L}_j} \right|^2 \quad (\text{A.4})$$

$$= S_{\text{cell}}(\mathbf{Q}) S_{\text{PBC}}(\mathbf{Q}) \quad (\text{A.5})$$

The advantage of this calculation is that it is linear in the sum of the number of particles N and the number of replicas M consider, $\mathcal{O}(N + M)$, much lower than the previous $\mathcal{O}(N^2 M^2)$. Consequently, if we want to focus in

a region of \mathbf{Q} , this new approach will be useful[45]. We are left with only one detail, respecting to the *powder average*. It is not trivial how to calculate this integral, since we need to give proper weights to each angle. In this work we used the Lebedev quadrature [46], although other methods like Importance Sampling Montecarlo can be useful in this situation.

ACKNOWLEDGMENTS

This work was partially supported by grants from AN-PCyT (PICT-2013-1692), CONICET and UBACyT.

-
- [1] D. Page, J. M. Lattimer, M. Prakash, and A. W. Steiner, *ApJS* **155**, 623 (2004).
 - [2] U. Geppert, M. K  ker, and D. Page, *Astronomy & Astrophysics* **426**, 11 (2004).
 - [3] S. Woosley and T. Janka, *Nature Physics* **1**, 147 (2005).
 - [4] D. G. Ravenhall, C. J. Pethick, and J. R. Wilson, *Phys. Rev. Lett.* **50**, 2066 (1983).
 - [5] M.-a. Hashimoto, H. Seki, and M. Yamada, *Prog. Theor.*

- Phys.* **71**, 320 (1984).
- [6] Y. Mochizuki and T. Izuyama, *The Astrophysical Journal* **440**, 263 (1995).
- [7] C. J. Horowitz, M. A. P  rez-Garc  a, and J. Piekarewicz, *Phys. Rev. C* **69**, 045804 (2004).
- [8] R. D. Williams and S. E. Koonin, *Nuclear Physics A* **435**, 844 (1985).
- [9] K. Oyamatsu, *Nuclear Physics A* **561**, 431 (1993).

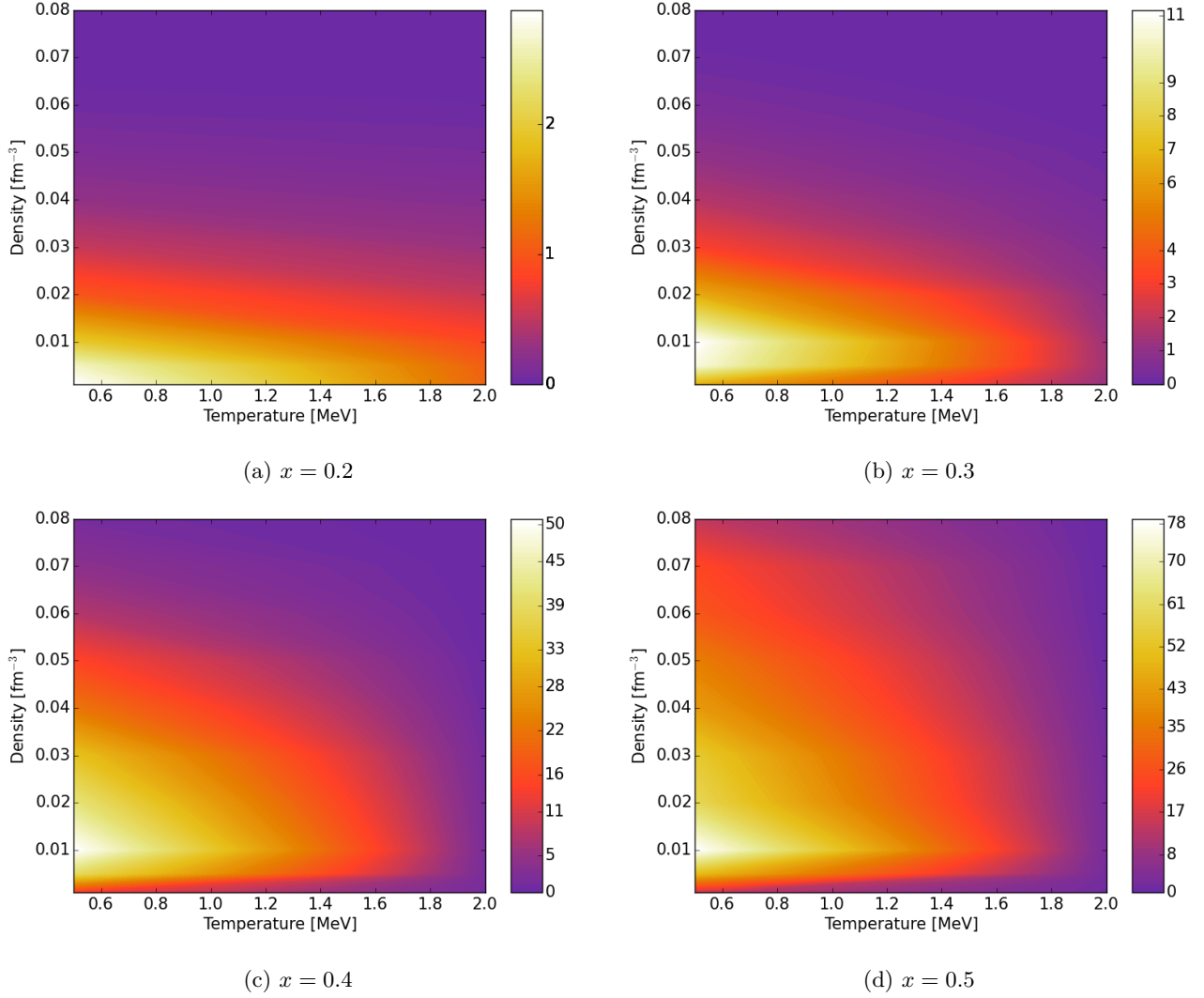


Figure 9: (Color online) Absorption peak in the Urca wavelength for different proton fractions as a function of temperature and density. It can be seen that the absorption decreases drastically for $T \gtrsim 0.8$ MeV. We also show here that the absorption is affected by the proton fraction, as can be noted by the scales on the color bar. Also note that the absorption for $x = 0.2$ and $x = 0.3$, the results are governed by noise.

- [10] C. P. Lorenz, D. G. Ravenhall, and C. J. Pethick, Phys. Rev. Lett. **70**, 379 (1993).
- [11] K. S. Cheng, C. C. Yao, and Z. G. Dai, Phys. Rev. C **55**, 2092 (1997).
- [12] G. Watanabe, K. Iida, and K. Sato, Nuclear Physics A **676**, 455 (2000).
- [13] G. Watanabe and K. Iida, Phys. Rev. C **68**, 045801 (2003).
- [14] K. Nakazato, K. Oyamatsu, and S. Yamada, Phys. Rev. Lett. **103**, 132501 (2009).
- [15] T. Maruyama, K. Niita, K. Oyamatsu, T. Maruyama, S. Chiba, and A. Iwamoto, Phys. Rev. C **57**, 655 (1998).
- [16] T. Kido, T. Maruyama, K. Niita, and S. Chiba, Nuclear Physics A **663–664**, 877c (2000).
- [17] G. Watanabe, K. Sato, K. Yasuoka, and T. Ebisuzaki, Phys. Rev. C **68**, 035806 (2003).
- [18] C. Horowitz, M. Pérez-García, J. Carriere, D. Berry, and J. Piekarewicz, Phys. Rev. C **70**, 065806 (2004).
- [19] C. O. Dorso, P. A. Giménez Molinelli, and J. A. López, Phys. Rev. C **86**, 055805 (2012).
- [20] P. N. Alcain, P. A. Giménez Molinelli, and C. O. Dorso, Phys. Rev. C **90**, 065803 (2014).
- [21] R. J. Lenk, T. J. Schlagel, and V. R. Pandharipande, Phys. Rev. C **42**, 372 (1990).
- [22] C. Dorso and J. Randrup, Physics Letters B **215**, 611 (1988).
- [23] A. Chernomoretz, L. Gingras, Y. Larochelle, L. Beaulieu, R. Roy, C. St-Pierre, and C. O. Dorso, Phys. Rev. C **65**, 054613 (2002).
- [24] J. A. López and C. Dorso, *Lectures Notes on Phase Transformations in Nuclear Matter* (WORLD SCIENTIFIC, 2000).
- [25] A. Barranon, C. O. Dorso, and J. A. Lopez, Revista mexicana de física **47**, 93 (2001).

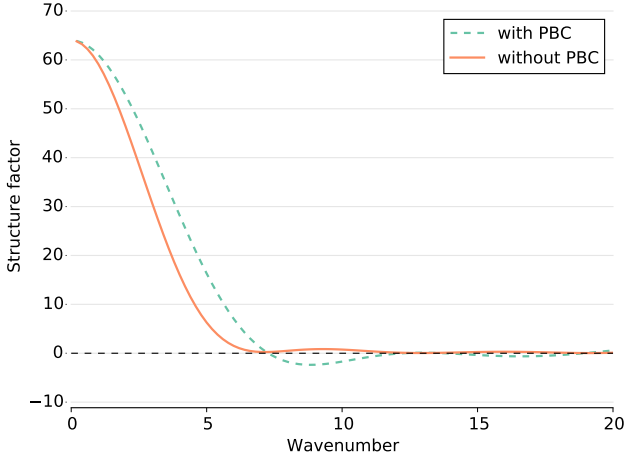


Figure 10: Comparison of structure factor with and without PBC. It's evident that the structure factor calculated with periodic boundary conditions shows negative values, which should not exist from the definition of the structure factor.

- [26] C. O. Dorso and J. A. López, Phys. Rev. C **64**, 027602 (2001).
- [27] A. Barrañón, R. Cárdenas, C. O. Dorso, and J. A. López, APH N.S., Heavy Ion Physics **17**, 59 (2003).
- [28] A. Barrañón, C. O. Dorso, and J. A. López, Nuclear Physics A **791**, 222 (2007).
- [29] A. Barrañón, J. Roa, and J. López, Phys. Rev. C **69**, 014601 (2004).
- [30] C. O. Dorso, C. R. Escudero, M. Ison, and J. A. López, Phys. Rev. C **73**, 044601 (2006).
- [31] C. A. Dorso, P. A. G. Molinelli, and J. A. López, J. Phys. G: Nucl. Part. Phys. **38**, 115101 (2011).
- [32] S. Plimpton, Journal of Computational Physics **117**, 1 (1995).
- [33] W. M. Brown, A. Kohlmeier, S. J. Plimpton, and A. N. Tharrington, Computer Physics Communications **183**, 449 (2012).
- [34] A. L. Fetter and J. D. Walecka, *Quantum Theory of Many-particle Systems* (Courier Dover Publications, 2003).
- [35] P. N. Alcain, P. A. Giménez Molinelli, J. I. Nichols, and C. O. Dorso, Phys. Rev. C **89**, 055801 (2014).
- [36] C. Dorso and J. Randrup, Physics Letters B **301**, 328 (1993).
- [37] C. O. Dorso and P. E. Balonga, Phys. Rev. C **50**, 991 (1994).
- [38] H. Childs, E. S. Brugger, K. S. Bonnell, J. S. Meredith, M. Miller, B. J. Whitlock, and N. Max, in *Proceedings of IEEE Visualization 2005* (Minneapolis, Minnesota, 2005) pp. 190–198.
- [39] H. Sonoda, G. Watanabe, K. Sato, T. Takiwaki, K. Yasuoka, and T. Ebisuzaki, Phys. Rev. C **75**, 042801 (2007).
- [40] M. Ruffert, H.-T. Janka, and G. Schaefer, arXiv:astro-ph/9509006 (1995), arXiv: astro-ph/9509006.
- [41] A. Mezzacappa, A. C. Calder, S. W. Bruenn, J. M. Blondin, M. W. Guidry, M. R. Strayer, and A. S. Umar, ApJ **495**, 911 (1998).
- [42] M. Liebendörfer, M. Rampp, H.-T. Janka, and A. Mezzacappa, ApJ **620**, 840 (2005).
- [43] T. Egami and S. J. L. Billinge, *Underneath the Bragg Peaks, Volume 16: Structural Analysis of Complex Materials*, 1st ed. (Pergamon, 2003).
- [44] Even further, now the imaginary part of $S(Q)$ is no longer zero.
- [45] We should consider though that in this approach, we will need $\mathcal{O}(N + M)$ calculations for each \mathbf{Q} , so we can't use it to sweep the whole \mathbf{Q} spectrum.
- [46] V. I. Lebedev, USSR Computational Mathematics and Mathematical Physics **15**, 44 (1975).